Submitted to Wave Motion in December, 2008

A direct relationship between bending waves and edge conditions of floating plates

Hyuck Chung and Colin Fox *

Abstract

Ocean waves travel deep into ice fields in the polar regions, both affecting the formation of sea-ice and causing its breakup. Recently, it has been shown that a relatively simple linear water and bending wave theory can predict the decay rate of the wave energy travelling through fractured ice sheets and floes at the geophysically important wave periods of 6 to 15 seconds. That work used simple free-edge conditions. A possible improvement to the current model is to better represent the effective connection due to partially frozen cracks that occur in practice. The Wiener-Hopf technique gives explicit formulae for the velocity potential and surface deflection, expressed as series expansions over the modes of the elastic plate floating on water of finite depth, with the coefficients in the expansion given as functions of four constants. These constants are determined by a system of four linear equations, represented by a 4-by-4 matrix and a 4-element vector. The elements of the matrix are given as explicit functions of relationship between edge conditions. General connections between ice sheets may be interpreted as a vertical and a rotational spring providing transition conditions for the shear force and the bending moment. The reflection and the transmission of waves can then be simply calculated as direct functions of the connection conditions. Conversely, reflected and transmitted waves allow complete characterization of the effective connection conditions at a material discontinuity.

1 Introduction

We consider two boundary value problems: a semi-infinite plate occupying one half of the water surface and two semi-infinite plates occupying the entire surface. The single-plate problem is actually a limiting case of the two-plate problem, and can be treated in the same way as the two-plate problem. We derive the analytic solution of the two-plate problem using the Wiener-Hopf (W-H) technique. The method of solution incorporates the boundary conditions at the edges of the plates into the solution formulae solely through a 4×4 matrix and 4-element column vector, which represents the connection between the two plates. The conditions that describe the connection are represented by two parameters. These parameters appear explicitly in the matrix defining boundary conditions, and are effectively spring constants in the connection.

In recent years, there has been significant progress made in the field of analytic or semi-analytic solutions of the fluid-loaded elastic plate problems. In particular, several researchers ([1, 6, 19]) have used the W-H technique to solve fluid-loaded plate problems as models for sea-ice dynamics. The W-H technique was first applied to a problem of ocean waves in sea-ice by Evans and Davies [5], though they did not give their solution in

*Department of Physics, University of Otago, PO Box 56, Dunedin, New Zealand

a form suitable for numerical computation. Although the researches in Russia may not be well known outside Russia, the papers by Goldstein and Marchenko, and Tkacheva [10, 13, 17] presented significant advances.

The formation and break-up of ice sheets in the polar regions has significant effect on marine life and ocean current dynamics. It has been observed by Squire et. al. [16] that ocean waves are one of the main causes of break-up of the ice sheets. Therefore, it has become important to know how much wave energy is how far into the ice fields. Kohout and Meylan [11] give a unique study, comparing field measurements to the theoretical results from the linear hydro-elasticity theory. Their conclusion is encouraging in the sense that linear theory has its place in describing actual sea-ice dynamics. It gives a good motivation for constructing a better model for waves in ice sheets using linear hydro-elasticity. We focus on the interaction between two ice sheets. Kohout and Meylan used free-edge conditions in their study. It is uncertain how to describe the physical conditions between two ice sheet because they are naturally as complex as the ice itself. In this paper we characterize the full range of transition conditions that can occur in a linear theory and find that only four physical parameters including the characteristic lengths are needed.

It has been previously established that the velocity potential of the water can be expressed by series expansions over the modes of the plate-covered water. When the coordinates are defined as shown in figure 1, the solutions in $y < 0$ and $y > 0$ are

$$\phi(x, y, z, t) = \sum_{n=-2}^{\infty} a_n e^{\mathrm{i}(kx+\kappa'_n y+\omega t)} \cosh \kappa_n (z + H), \text{ for } y < 0$$

$$\phi(x, y, z, t) = \sum_{n=-2}^{\infty} b_n e^{\mathrm{i}(kx+\mu'_n y+\omega t)} \cosh \mu_n (z + H), \text{ for } y > 0$$

where κ_n, κ'_n, μ_n and μ'_n are the wavenumbers for each mode and ω is the radial frequency of the incident wave. In this paper the coefficients a_n and b_n will be determined by a rather lengthy process using the W-H technique. In section 4 explicit formulae for a_n and b_n will be given as functions of four constants, (d_0, d_1, d_2, d_3). These constants are computed by solving a linear equation of form

$$\mathbf{T}_{\sigma_1,\sigma_2} \begin{pmatrix} d_0 \\ d_1 \\ d_2 \\ d_3 \end{pmatrix} = \mathbf{v}$$

where $\mathbf{T}_{\sigma_1,\sigma_2}$ is a 4×4 matrix and $\mathbf{v}$ is a 4-element column vector. Connection between the ice sheets is equivalent to linking them with a vertical and a rotational spring with spring constants σ_1 and σ_2, which appear explicitly in $\mathbf{T}_{\sigma_1,\sigma_2}$. Therefore, one does not have to go through the W-H solution procedure to compute the solution for each specific edge condition or connection between them. Instead, the simplified procedure given in section 5 provides a simple and exact relationship.

2 Formulation of the boundary value problems

2.1 Governing equations

We first formulate the governing equations in physical dimensions, then convert them to a non-dimensional form using the characteristic length and time in the following subsection.

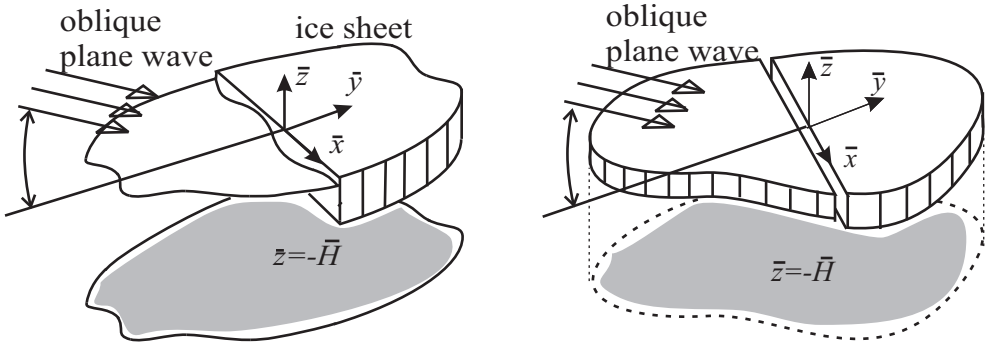

Figure 1: Schematic drawings of a plane wave obliquely incident at the water-plate and plate-plate transition. The origin of the coordinate system is placed at the surface transition.

The geometry of the two problems are shown in figure 1. The motion of the fluid is parameterized by a velocity potential, $\bar{\phi}$, which satisfies Laplace's equation with a solid bottom condition,

$$\nabla^2_{\bar{x},\bar{y},\bar{z}}\bar{\phi}\left(\bar{x},\bar{y},\bar{z}\right)=0,\ -\infty<\bar{x},\bar{y}<\infty,-\bar{H}<\bar{z}<0 \tag{1}$$

$$\bar{\phi}_{\bar{z}}\big|_{\bar{z}=-\bar{H}}=0,\quad -\infty<\bar{x},\bar{y}<\infty. \tag{2}$$

Here $\nabla^2_{\bar{x},\bar{y},\bar{z}}$ denotes the Laplacian in the three space dimensions while $\bar{\phi}_{\bar{z}}$ denotes the partial derivative of $\bar{\phi}$ in the $\bar{z}$ direction. We will use analogous subscript notation for other partial derivatives. In the ice-covered region, $\bar{y}>0$, the vertical displacement $\bar{\eta}\left(\bar{x},\bar{y}\right)$ of the ice sheet satisfies the Kirchhoff thin-plate equation

$$D\nabla^4_{\bar{x},\bar{y}}\bar{\eta}+\bar{m}\left(\bar{\eta}_{\bar{t}\bar{t}}+g\right)=\bar{p}\quad\text{for}\quad -\infty<\bar{x}<\infty,0<\bar{y}<\infty \tag{3}$$

and is related to the potential by the linearized Bernoulli equation

$$\rho\bar{\phi}_{\bar{t}}+\rho g\bar{\eta}+\bar{p}=0, \tag{4}$$

where D is the flexural rigidity of the ice sheet, $\bar{m}\left(=\rho_{\mathrm{i}}h\right)$ is mass per unit surface area of the ice sheet (ρ_{i} is the density of sea ice), $\bar{p}$ is the pressure acting at the lower surface of the ice sheet, and ρ is density of water. Here $\nabla^4_{\bar{x},\bar{y}}$ is the biharmonic operator in the plane of the ice sheet. The flexural rigidity D is usually related to the effective Young's modulus E and Poisson's ratio ν by the relation $D=Eh^3/12\left(1-\nu^2\right)$. The assumption that no cavitation occurs between the ice sheet and water, gives the kinematic condition that

$$\bar{\phi}_{\bar{z}}\big|_{\bar{z}=0}=\bar{\eta}_{\bar{t}}\quad\text{for}\quad\bar{y}>0 \tag{5}$$

while the velocity potential in the free-surface region satisfies

$$\bar{\phi}_{\bar{t}\bar{t}}\big|_{\bar{z}=0}+g\,\bar{\phi}_{\bar{z}}\big|_{\bar{z}=0}=0\quad\text{for}\quad\bar{y}<0. \tag{6}$$

We can formulate the two plate case simply by replacing the free surface condition (6) with a plate equation, giving the two plate equations

$$D_1\nabla^4_{\bar{x},\bar{y}}\bar{\eta}+\bar{m}_1\left(\bar{\eta}_{\bar{t}\bar{t}}+g\right)=\bar{p}\quad\text{for}\quad -\infty<\bar{x}<\infty,-\infty<\bar{y}<0,$$

$$D_2\nabla^4_{\bar{x},\bar{y}}\bar{\eta}+\bar{m}_2\left(\bar{\eta}_{\bar{t}\bar{t}}+g\right)=\bar{p}\quad\text{for}\quad -\infty<\bar{x}<\infty,0<\bar{y}<\infty.$$

The subscript 1 and 2 will indicate the parameters for the plate in $\bar{y}<0$ and $\bar{y}>0$, respectively.

2.2 Non-dimensional formulation

The system of equations introduced in subsection 2.1 can be non-dimensionalized by scaling variables using the characteristic length l and time τ defined by

$$l = \sqrt[4]{\frac{D}{\rho g}}, \quad \tau = \sqrt{\frac{l}{g}}.$$

The dimensionless quantities (without over-bar) are

$$\begin{array}{ccc} (x,y,z) = (\bar{x},\bar{y},\bar{z})/l, & t = \bar{t}/\tau, & \omega = \bar{\omega}\tau, \\ \eta = \bar{\eta}/l, & \phi = \bar{\phi}/\left(l\sqrt{gl}\right), & \\ p = \bar{p}/\left(\rho g l\right), & m = \bar{m}/\left(\rho l\right). & \end{array}$$

This scaling is optimal in the sense that it captures significant physical properties of the response of the system and hence the number of solutions required is reduced to a minimal, canonical, set (see [7]).

The equations for the non-dimensional velocity potential become, from equations from (1) to (6),

$$\begin{array}{lll} \left(\nabla^4_{x,y} + m\dfrac{\partial^2}{\partial t^2} + 1\right)\phi_z + \phi_{tt} = 0 & \text{for} & z = 0, y > 0, \\ \nabla^2_{x,y,z}\phi = 0 & \text{for} & -\infty < x, y < \infty, -H < z < 0, \\ \phi_z = 0 & \text{for} & z = -H, \\ \phi_{tt} = -\phi_z & \text{for} & z = 0, y < 0. \end{array}$$

We use the same non-dimensionalization procedure for the two-plate problem. The two plate equations are non-dimensionalized using the characteristic length of the plate in $y > 0$, denoted l_2, to give

$$\begin{array}{l} \left(l_{\mathrm{r}}^4\nabla^4_{x,y} + m_1\dfrac{\partial^2}{\partial t^2} + 1\right)\phi_z + \phi_{tt} = 0 \quad \text{for} \quad z = 0, y < 0, \\ \left(\nabla^4_{x,y} + m_2\dfrac{\partial^2}{\partial t^2} + 1\right)\phi_z + \phi_{tt} = 0 \quad \text{for} \quad z = 0, y > 0, \end{array}$$

where l_{r} is the ratio of the two characteristic lengths, $l_{\mathrm{r}} = l_1/l_2$. The non-dimensional mass densities are defined as

$$m_1 = \frac{\bar{m}_1}{\rho l_2}, \quad m_2 = \frac{\bar{m}_2}{\rho l_2}.$$

Notice that the equation for $y < 0$ reduces to that for the water surface, when $l_1 = 0$. Hence, we will only deal with the two-plate problem in the following sections.

2.3 Boundary conditions

A plate floating without any constraints at the boundary satisfies the two natural boundary conditions (see Shames and Dym [15]),

$$\left.\begin{array}{c} \phi_{zyy} + \nu\phi_{zxx} = 0 \\ \nabla^2_{x,y}\phi_{zy} + (1-\nu)\,\phi_{zyxx} = 0 \end{array}\right\} \text{ for } y = 0+, z = 0.$$

However additional conditions are required when the two plates are mechanically connected. The most general conditions can be derived from the variational calculus shown

in section 6.4 of [15] and are necessarily a linear relationship between the following derivatives across the boundary:

$$B_1\eta|_{y=0-} = l_{\mathrm{r}}^4 \left\{ \eta_{yyy}|_{y=0-} - k^2\,(2-\nu)\,\eta_y|_{y=0-} \right\},$$
$$B_1\eta|_{y=0+} = \eta_{yyy}|_{y=0+} - k^2\,(2-\nu)\,\eta_y|_{y=0+},$$

which are shear forces,

$$B_2\eta|_{y=0-} = l_{\mathrm{r}}^4 \left(\eta_{yy}|_{y=0-} - k^2\nu\,\eta|_{y=0-} \right),$$
$$B_2\eta|_{y=0+} = \eta_{yy}|_{y=0+} - k^2\nu\,\eta|_{y=0+},$$

which are bending moments, the displacement $\eta|_{y=0\pm}$, and the slope $\eta_y|_{y=0\pm}$. B_1 and B_2 denote the boundary operators that give shear force and bending moment at the edge of the plate, respectively.

3 Method of solution

As depicted in figure 1, we assume that the plates are excited by a single frequency plane wave with x and t dependence given by $\exp \mathrm{i}\,(kx+\omega t)$. The wave number k is determined by the travelling wave number in the region $y<0$ denoted κ_0 and the incident angle, θ, i.e., $k=\kappa_0 \sin\theta$. Therefore the velocity potential $\phi\,(x,y,z,t)$ can be rewritten using a complex valued function $\phi\,(y,z)$ as

$$\phi\,(x,y,z,t) = \mathrm{Re}\left[\phi\,(y,z)\,e^{\mathrm{i}(kx+\omega t)}\right].$$

The complex potential $\phi\,(y,z)$ then satisfies Helmholtz equation

$$\left(\frac{\partial^2}{\partial y^2} + \frac{\partial^2}{\partial z^2} - k^2\right)\phi = 0 \quad \text{for} \quad -\infty < y < \infty, -H < z < 0 \tag{7}$$

with the boundary condition at the bottom of the sea

$$\phi_z|_{z=-H} = 0. \tag{8}$$

The linearity of the system enables the rest of the equations to be rewritten without the x and t dependence. We then have the following equations at the surface.

$$\left(l_{\mathrm{r}}^4\left(\frac{\partial}{\partial y^2} - k^2\right)^2 - m_1\omega^2 + 1\right)\phi_z = \omega^2\phi \ \text{ for } y<0, \tag{9}$$

$$\left(\left(\frac{\partial}{\partial y^2} - k^2\right)^2 - m_2\omega^2 + 1\right)\phi_z = \omega^2\phi \ \text{ for } y>0. \tag{10}$$

3.1 Modal expansion of the solution

The solution of the system given by (7) and (8) can be found using the method of separation of variables. This gives modes of the form

$$\phi\,(y,z) \sim e^{\pm \mathrm{i}\,\alpha y}\cosh\gamma\,(z+H) \tag{11}$$

where $\gamma^2 = \alpha^2 + k^2$. We can derive the algebraic equations for the spatial wave numbers κ and μ by substituting the eigenfunction (11) into (9) and (10). The resulting algebraic equations

$$f_1(\gamma) = l_{\mathrm{r}}^4\gamma^4 - m_1\omega^2 + 1 - \frac{\omega^2}{\gamma \tanh \gamma H} = 0 \tag{12}$$

and

$$f_2(\gamma) = \gamma^4 - m_2\omega^2 + 1 - \frac{\omega^2}{\gamma \tanh \gamma H} = 0 \tag{13}$$

are called the dispersion equations and have an infinite number of roots in the complex plane. Equation (12) has two real, four complex and infinite number of pure imaginary roots, which we denote $\pm\kappa_0$, $\{\pm\kappa_{-1}, \pm\kappa_{-2}\}$ and $\pm\kappa_n$, $n = 1, 2, ...$, respectively. Equation (13) also has two real, four complex and infinite number of pure imaginary roots, which we denote $\pm\mu_0$, $\{\pm\mu_{-1}, \pm\mu_{-2}\}$ and $\pm\mu_n$, $n = 1, 2, ...$ Note that $\mu_{-1} = -\mu_{-2}^*$. Note that (12) becomes the water-surface dispersion equation when $l_{\mathrm{r}}^4 = 0$, in which case there are no complex roots. Numerical computation of the roots of the dispersion equations is detailed in [8].

The complete solution of the boundary problem is then expressed by a sum over all the permissible roots (see [12] for a rigorous proof). The velocity potential for $y < 0$ with free surface is

$$\phi(y, z) = \left(Ie^{\mathrm{i}\,\kappa_0' y} + Re^{-\mathrm{i}\,\kappa_0' y}\right) \frac{\cosh \kappa_0 (z + H)}{\kappa_0 \sinh \kappa_0 H} + \sum_{n=1}^{\infty} a_n e^{-\mathrm{i}\,\kappa_n' y} \frac{\cosh \kappa_n (z + H)}{\kappa_n \sinh \kappa_n H}$$

and with an ice sheet is

$$\phi(y, z) = \left(Ie^{\mathrm{i}\,\kappa_0' y} + Re^{-\mathrm{i}\,\kappa_0' y}\right) \frac{\cosh \kappa_0 (z + H)}{\kappa_0 \sinh \kappa_0 H} + \sum_{\substack{n=-2 \\ n\neq 0}}^{\infty} a_n e^{-\mathrm{i}\,\kappa_n' y} \frac{\cosh \kappa_n (z + H)}{\kappa_n \sinh \kappa_n H},$$

while the velocity potential for $y > 0$ with the ice sheet is

$$\phi(y, z) = Te^{\mathrm{i}\,\mu_0' y} \frac{\cosh \mu_0 (z + H)}{\mu_0 \sinh \mu_0 H} + \sum_{\substack{n=-2 \\ n\neq 0}}^{\infty} b_n e^{\mathrm{i}\,\mu_n' y} \frac{\cosh \mu_n (z + H)}{\mu_0 \sinh \mu_0 H}.$$

The surface velocities are derived by the z-derivatives of the above potentials. We here give only the plate-covered surface velocities

$$\phi_z(y, 0) = \left(Ie^{\mathrm{i}\,\kappa_0' y} + Re^{-\mathrm{i}\,\kappa_0' y}\right) + \sum_{\substack{n=-2 \\ n\neq 0}}^{\infty} a_n e^{-\mathrm{i}\,\kappa_n' y}, \text{ for } y < 0$$

$$\phi_z(y, 0) = Te^{\mathrm{i}\,\mu_0' y} + \sum_{\substack{n=-2 \\ n\neq 0}}^{\infty} b_n e^{\mathrm{i}\,\mu_n' y}, \text{ for } y > 0.$$

The transmission, reflection, and incident amplitudes denoted by T, R and I are quantities that we use to visualize the waves in the sea-ice. These quantities are the far-field wave amplitudes that can be measured in the field. The wavenumbers κ_n' and μ_n' are wave numbers projected onto the y axis and related to the roots of the dispersion equations by

$$\kappa_n' = \sqrt{\kappa_n^2 - k^2}, \quad \mu_n' = \sqrt{\mu_n^2 - k^2}.$$

The branch of the square root has been chosen so that the primed variables equal the unprimed roots when $k = 0$.

3.2 Derivation of the solution using the W-H technique

This section briefly describes the derivation of the solution of the system of equations given in the previous section using the W-H technique. We apply the Fourier transform to the differential equations of ϕ in the respective domains $y < 0$ and $y > 0$, defined as

$$\Phi_+(\alpha, z) = \int_0^\infty \phi(y, z)\, e^{\mathrm{i}\,\alpha y} dy, \quad \Phi_-(\alpha, z) = \int_{-\infty}^0 \phi(y, z)\, e^{\mathrm{i}\,\alpha y} dy. \tag{14}$$

We also denote the same transforms of $\phi_z(y, 0)$ in $y > 0$ and $y < 0$ by $\Phi'_+(\alpha)$ and $\Phi'_-(\alpha)$, respectively. From the transforms of Laplace's equation and the condition at $z = -H$, we have

$$\Phi_\pm(\alpha, z) = \Phi_\pm(\alpha, 0)\, \frac{\cosh\gamma(z + H)}{\cosh\gamma H} \pm g(\alpha, z) \tag{15}$$

where $\gamma = \sqrt{\alpha^2 + k^2}$ and $g(\alpha, z)$ is a regular function determined by the contribution from the boundary, $\{\phi_y(0, z) - \mathrm{i}\,\alpha\phi(0, z)\}$. Note that $\mathrm{Re}\,\gamma > 0$ when $\mathrm{Re}\,\alpha > 0$ and $\mathrm{Re}\,\gamma < 0$ when $\mathrm{Re}\,\alpha < 0$. Also the functions $\Phi_+(\alpha, z)$ and $\Phi_-(\alpha, z)$ are regular in $\mathrm{Im}\,\alpha > 0$ and $\mathrm{Im}\,\alpha < 0$, respectively. We have, by differentiating both sides of (15) with respect to z at $z = 0$,

$$\Phi'_\pm(\alpha) = \Phi_\pm(\alpha, 0)\,\gamma\tanh\gamma H \pm g_z(\alpha, 0) \tag{16}$$

where $\Phi'_\pm(\alpha)$ is the z-derivative of $\Phi_\pm(\alpha, z)$ at $z = 0$.

Applying the same integral transforms (14) to the plate equations for $y < 0$ and $y > 0$ and using (16), we obtain

$$f_1(\gamma)\,\Phi'_-(\alpha) + C_1(\alpha) = 0, \tag{17}$$

$$f_2(\gamma)\,\Phi'_+(\alpha) + C_2(\alpha) = 0, \tag{18}$$

where

$$C_1(\alpha) = -\frac{\rho\omega^2 g_z(\alpha, 0)}{\gamma\tanh\gamma H} + P_1(\alpha), \quad C_2(\alpha) = \frac{\rho\omega^2 g_z(\alpha, 0)}{\gamma\tanh\gamma H} - P_2(\alpha).$$

and P_j, $j = 1, 2$, are second order polynomials of α. Notice that f_1 and f_2 are the dispersion equations (12) and (13).

The functions $\Phi'_-(\alpha)$, and $\Phi'_+(\alpha)$ are defined for $\mathrm{Im}\,\alpha < 0$ and $\mathrm{Im}\,\alpha > 0$ respectively, however they can be extended to the whole plane using (17) and (18) as definitions for analytic continuation. Equations (17) and (18) show that the singularities of Φ'_- and Φ'_+ are determined by the positions of the zeros of f_1 and f_2, since $g_z(\alpha, 0)$ is bounded and zeros of $\gamma\tanh\gamma H$ are not singularities of $\Phi'_\pm$. The two functions $\Phi'_-(\alpha)$ and $\Phi'_+(\alpha)$ do not share domains of regularity, because they are separated by the real axis. We are able to manipulate the regions of regularity by including or removing one singular part of the functions. Here, we remove a singular part corresponding to $-\kappa'_0$, which gives rise to the incident wave, from $\Phi'_-(\alpha)$ and from $\Phi'_+(\alpha)$. The modified functions denoted by $\Psi'_\pm(\alpha)$ satisfy

$$f_1(\gamma)\,\Psi'_-(\alpha) + C_1(\alpha) = 0, \tag{19}$$

$$f_2(\gamma)\,\Psi'_+(\alpha) - \frac{\tilde{I} f_2(\kappa'_0)}{\alpha + \kappa'_0} + C_2(\alpha) = 0, \tag{20}$$

where $\tilde{I}$ is the amplitude associated with κ'_0. The modified functions $\Psi'_-(\alpha)$ and $\Psi'_+(\alpha)$ do have a common strip region of analyticity on the real axis with the indentations over

$-\kappa_0'$, $-\mu_0'$ and under κ_0', μ_0' as shown in figure 8. Let $\mathcal{D}_+$ and $\mathcal{D}_-$ denote the upper and lower half of the α-plane that are sharing the indented region on the real axis described above and shown in figure 8. Then, we may now add both sides of (19) and (20) to derive a typical W-H equation defined in $\mathcal{D}_+ \cap \mathcal{D}_-$,

$$f_1(\gamma)\,\Psi_-'(\alpha) + f_2(\gamma)\,\Psi_+'(\alpha) - \frac{\tilde{I} f_2(\kappa_0')}{\alpha + \kappa_0'} + C(\alpha) = 0 \tag{21}$$

where $C = C_1 + C_2$.

The standard method of solution of the W-H equation requires factorization of the two dispersion functions. Weierstrass' factor theorem and the symmetry of the positions of the roots in S_1 and S_2, sets of roots of f_1 and f_2 in $\mathcal{D}_+$, respectively, give

$$\frac{f_2}{f_1} = K(\alpha)\,K(-\alpha), \quad K(\alpha) = \left(\prod_{q' \in S_1} \frac{q}{q'+\alpha}\right)\left(\prod_{q' \in S_2} \frac{q'+\alpha}{q}\right).$$

Note that $K(\alpha)$ is regular in the upper half plane and on the real axis except at $-\kappa_0'$ and $-\mu_0'$ and the infinite products converge in the order of q^{-5} as $|q|$ becomes large. Then (21) can be rewritten as

$$\begin{aligned} &K(\alpha)\left[f(\gamma)\,\Psi_+'(\alpha) + C\right] - \left(K(\alpha) - \frac{1}{K(\kappa_0')}\right)\frac{\tilde{I} f_2(\kappa_0)}{\alpha + \kappa_0'} \\ &\quad = -\frac{1}{K(-\alpha)}\left[f(\gamma)\,\Psi_-'(\alpha) - C\right] - \left(\frac{1}{K(-\alpha)} - \frac{1}{K(\kappa_0')}\right)\frac{\tilde{I} f_2(\kappa_0)}{\alpha + \kappa_0'} \end{aligned} \tag{22}$$

where $f(\gamma) = f_2(\gamma) - f_1(\gamma)$. The splitting is actually performed on $f_1 \gamma \sinh \gamma H$ and $f_2 \gamma \sinh \gamma H$, which are not zero at $\gamma = 0$.

The left hand side of (22) is regular in $\mathcal{D}_+$ and the right hand side is regular in $\mathcal{D}_-$. Notice that a function is added to both sides of the equation to make the right hand side of the equation regular in $\mathcal{D}_-$. The left hand side of (22) is $o(\alpha^4)$ as $|\alpha| \to \infty$ in $\mathcal{D}_+$, since $\Psi_+' \to 0$ and $K(\alpha) = O(1)$ as $|\alpha| \to \infty$ in $\mathcal{D}_+$. The right hand side of (22) has the same analytic properties in $\mathcal{D}_-$. Then Liouville's theorem (see section 2.4 of [2]) tells us that there exists a function that we denote $J(\alpha)$, equal to both sides in (22) in the whole plane, that is a polynomial of degree three

$$J(\alpha) = d_0 + d_1\alpha + d_2\alpha^2 + d_3\alpha^3.$$

Application of Liouville's theorem is the key reduction in the W-H solution that allows writing coefficients $\{a_n\}$ and $\{b_n\}$ in terms of the four coefficients defining $J(\alpha)$.

Equating (22) for $\Psi' = \Psi_-' + \Psi_+'$ gives

$$\Psi'(\alpha) = \frac{-F(\alpha)}{K(\alpha)\,f_1(\gamma)} \text{ or } -\frac{K(-\alpha)\,F(\alpha)}{f_2(\gamma)}$$

where

$$F(\alpha) = J(\alpha) - \frac{\tilde{I} f_2(\gamma)}{(\alpha + \kappa_0')\,K(\kappa_0')}.$$

Notice that procedure we used in forming (22) eliminates the need of calculating C. We are now able to calculate solutions using the inverse Fourier transform

$$\phi_z(y,0) = \frac{1}{2\pi}\int_{-\infty}^{\infty} \Phi'(\alpha)\,e^{-\mathrm{i}\alpha y}\,d\alpha.$$

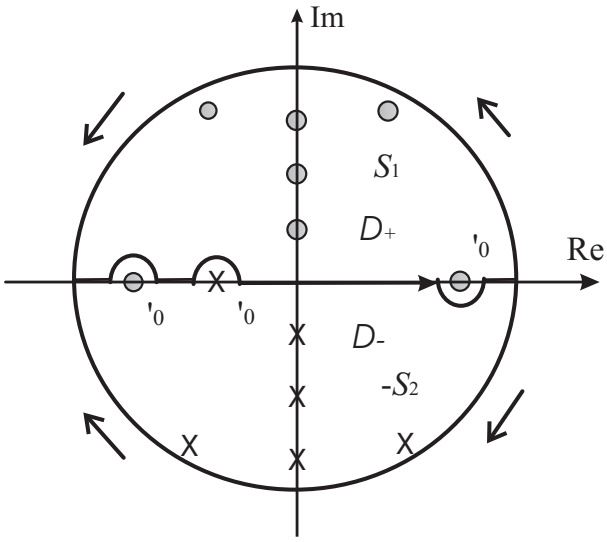

Figure 2: Schematics of the contour integration paths of the inverse Fourier transform and the positions (not to scale) of the corresponding roots in the α-plane. μ_0' is not shown since it is not a singularity of the integrand. The domains $\mathcal{D}_\pm$ have an overlapping region of analyticity consisting of an open region about the indented integral path. S_1 and S_2 denote the sets of the singularities in $\mathcal{D}_+$ and $\mathcal{D}_-$, respectively.

Solutions for $y < 0$ are evaluated by closing the contour of integration in $\mathcal{D}_+$ as depicted in figure 8. After putting back the incident wave, we have

$$\phi_z(y,0) = \mathrm{i}\,\tilde{I} e^{\mathrm{i}\,\kappa_0' y} - \sum_{q\in S_1} \frac{\mathrm{i}\,F(q')\,qR_1(q)}{q'K(q')} e^{-\mathrm{i}\,q' y}, \tag{23}$$

where the residue, $R_1(q)$, of $[f_1(\gamma)]^{-1}$ at $\gamma = q$ is given by

$$R_1(q) = \left(\left.\frac{df_1(\gamma)}{d\gamma}\right|_{\gamma=q}\right)^{-1} = \frac{\omega^2 q}{\left(5l_{\mathrm{r}}^4 q^4 + b_1\right)\omega^2 + H\left(\left(l_{\mathrm{r}}^4 q^5 + b_1 q\right)^2 - \omega^4\right)}. \tag{24}$$

It is important computationally that the above formula does not have the oscillating function $\tanh qH$, which has been removed using the dispersion equation. As a result, $|R_1(q)|$ decays monotonically and rapidly as $|q|$ increases. We also used $b_1 = -m_1\omega^2 + 1$ and $f_1(q) = 0$ to simplify the formula. The velocity potential $\phi(y,z)$ is explicitly, from (15) and (16),

$$\phi(y,z) = \frac{\mathrm{i}\,\tilde{I}\cosh\kappa_0(z+H)}{\kappa_0\sinh\kappa_0 H} e^{\mathrm{i}\,\kappa_0' y} - \sum_{q'\in S_1} \frac{\mathrm{i}\,F(q')\,R_1(q)\cosh q(z+H)}{q'K(q')\sinh qH} e^{-\mathrm{i}\,q' y}.$$

This formula gives coefficients $\{a_n\}$ explicitly. Notice that $\mathrm{i}\,\tilde{I} = I$.

For $y > 0$, we derive $\phi_z(y,0)$ and $\phi(y,z)$ by closing the contour of integration in $\mathcal{D}_-$ as depicted in figure 8,

$$\phi_z(y,0) = -\sum_{q'\in S_2} \frac{\mathrm{i}\,K(q')\,F(-q')\,qR_2(q)}{q'} e^{-\mathrm{i}\,q' y}, \tag{25}$$

$$\phi(y,z) = -\sum_{q'\in S_2} \frac{\mathrm{i}\,K(q')\,F(-q')\,R_2(q)\cosh q(z+H)}{q'\sinh qH} e^{-\mathrm{i}\,q' y},$$

where R_2 is a residue of $[f_2(\gamma)]^{-1}$ and its formula can be obtained by replacing the subscript 1 with 2 and l_r with 1 in (24). Notice that the coefficients of ϕ_z decay as $O(q^{-6})$ as $|q|$ becomes large, because $R_j \sim O(q^{-9})$, $j = 1, 2$. Thus the displacement is bounded up to the fourth y-derivatives. The coefficients of ϕ, have an extra $1/q' \tanh q'H \sim O(q^4)$. Hence the coefficients decay as $O(q^{-2})$ as $|q|$ becomes large. Therefore, ϕ is bounded everywhere including at $y = 0$.

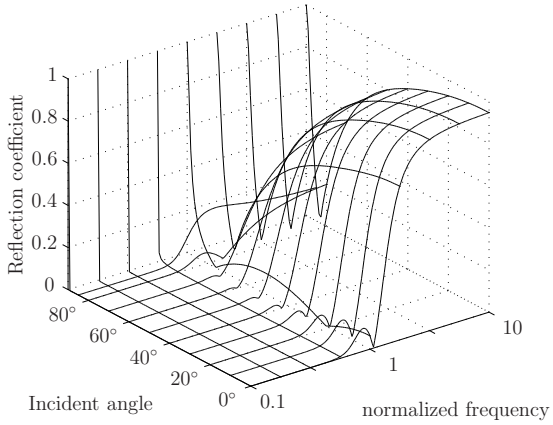

Figure 3: The reflection coefficient as a function of the incident angle (in degrees) and the non-dimensional radial frequency ω (log-scale) when $l_\mathrm{r} = 1$ and $H = 2\pi$.

Figure 3 shows an example of computation of the reflection coefficient as a function of frequency and incident angle for two sheets of equal thickness when the edges are free of constraints. Similar figures have been shown in several other papers introduced in section 1. Here, the figure shows that there are three regions of distinct behaviour of the reflection. At low-frequency (normalized frequency $\omega < 0.7$) there is no wave reflected, i.e., $R \simeq 0$. For high-frequency, $\omega > 4$, and shallow incident angle, $\theta < 30°$, there is total reflection, i.e., $R \simeq 1$. At mid-frequencies around unit normalized frequency or at steep incident angles, there is partial reflection.

4 Connection between the ice sheets

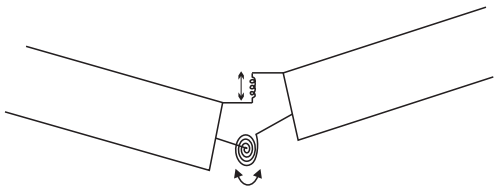

Figure 4: The rotational and the vertical springs connecting the two ice sheets.

In reality, the edges of the ice sheets may not be freely moving. Therefore the derivatives given in subsection 2.3 must satisfy the natural transition conditions for the shear force and the bending moment. Furthermore, the bending moment at the transition is determined by a rotational constraint due to the difference in the gradient at the boundary, and the shear force is determined by the vertical constraint due to the difference in the

vertical displacement. These constraints may be interpreted as the result of two springs, one in each of the vertical and the rotational directions as shown in figure 4. Then the displacement and the gradient are coupled with the shear force and the bending moment by the following equations.

$$\begin{aligned} \sigma_1 \left(\eta|_{y=0-} - \eta|_{y=0+} \right) &= \pm\, B_1 \eta|_{y=0\pm}\,, \\ \sigma_2 \left(\eta_y|_{y=0-} - \eta_y|_{y=0+} \right) &= \pm\, B_2 \eta|_{y=0\pm}\,, \end{aligned} \tag{26}$$

where σ_1 and σ_2 are the vertical and the rotational spring constants, respectively. In addition the following continuity conditions hold

$$B_1\, \eta|_{y=0-} = B_1\, \eta|_{y=0+}\,, \quad B_2\, \eta|_{y=0-} = B_2\, \eta|_{y=0+}\,. \tag{27}$$

Using (5), (23), and (25), the complex displacement η may be written as a linear sum over the coefficients $\{d_i\}$ defining $J(\alpha)$. That sum is

$$\eta(y) = \begin{cases} c_4^-(y) + \displaystyle\sum_{i=0}^{3} d_i c_i^-(y)\,, & \text{for } y < 0 \\ \\ c_4^+(y) + \displaystyle\sum_{i=0}^{3} d_i c_i^+(y)\,, & \text{for } y > 0 \end{cases} \tag{28}$$

where functions $c_i^{\pm}(y)$, $i = 0, 1, 2, 3$, have been explicitly determined and do not depend on the boundary conditions but do depend on characteristic length. For example, c_0^+ is

$$c_0^+(y) = -\frac{1}{\omega} \sum_{q' \in S_2} \frac{K(q')\, q R_2(q)}{q'} e^{-\mathrm{i}\, q' y}.$$

The boundary conditions can then be expressed as algebraic equations for the column vector $\mathbf{d} = (d_0, d_1, d_2, d_3)$. On substituting (28) into the boundary operators in section 2.3, the boundary values take the form

$$\begin{aligned} \eta|_{y=0\pm} = \mathcal{A}_1^{\pm} \cdot \mathbf{d} + \mathcal{B}_1^{\pm},\ \eta_y|_{y=0\pm} = \mathcal{A}_2^{\pm} \cdot \mathbf{d} + \mathcal{B}_2^{\pm}, \\ B_1 \eta_y|_{y=0\pm} = \mathcal{A}_3^{\pm} \cdot \mathbf{d} + \mathcal{B}_3^{\pm},\ B_2 \eta_y|_{y=0\pm} = \mathcal{A}_4^{\pm} \cdot \mathbf{d} + \mathcal{B}_4^{\pm}, \end{aligned}$$

where $\mathcal{A}_i^{\pm}$, $\mathcal{B}_i^{\pm}$, $i = 1, 2, 3, 4$ are row vectors and scalar values, respectively.

The boundary conditions in (26) and (27), which are linear equations with respect to η, give the matrix equation

$$\mathbf{T}_{\sigma_1,\sigma_2}\, \mathbf{d} = \mathbf{v}, \tag{29}$$

where $\mathbf{T}_{\sigma_1,\sigma_2}$ is the 4×4 matrix

$$\mathbf{T}_{\sigma_1,\sigma_2} = \begin{pmatrix} \sigma_1 \left(\mathcal{A}_1^- - \mathcal{A}_1^+ \right) - \mathcal{A}_3^+ \\ \sigma_2 \left(\mathcal{A}_2^- - \mathcal{A}_2^+ \right) - \mathcal{A}_4^+ \\ \mathcal{A}_3^- - \mathcal{A}_3^+ \\ \mathcal{A}_4^- - \mathcal{A}_4^+ \end{pmatrix} \tag{30}$$

and $\mathbf{v}$ the 4-element column vector

$$\mathbf{v} = \begin{pmatrix} -\mathcal{B}_1^- + \mathcal{B}_1^+ - \mathcal{B}_3^+ \\ -\mathcal{B}_2^- + \mathcal{B}_2^+ - \mathcal{B}_4^+ \\ -\mathcal{B}_3^- + \mathcal{B}_3^+ \\ -\mathcal{B}_4^- + \mathcal{B}_4^+ \end{pmatrix}.$$

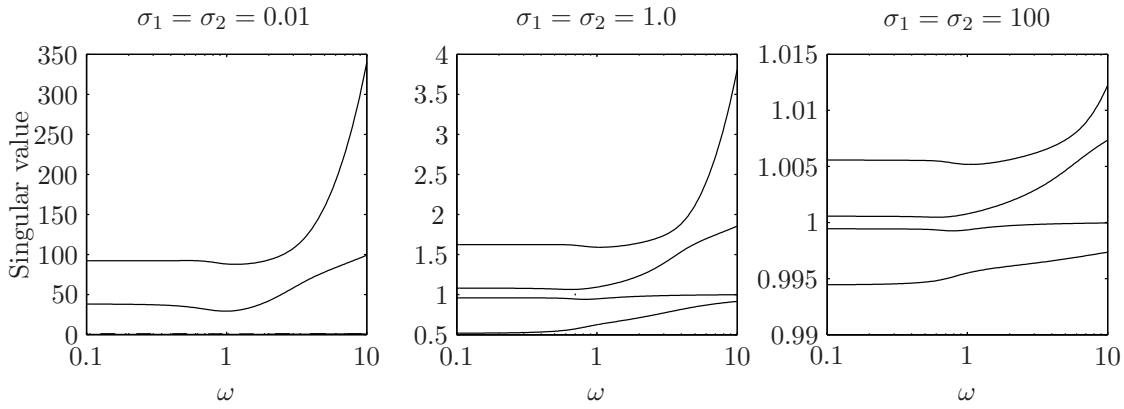

Figure 5: The singular values of the transition matrix against the frequency for various σ_1 and σ_2. The ω-axis is in log-scale. The water depth is 2π, the incident angle is zero and $l_\mathrm{r} = 1$.

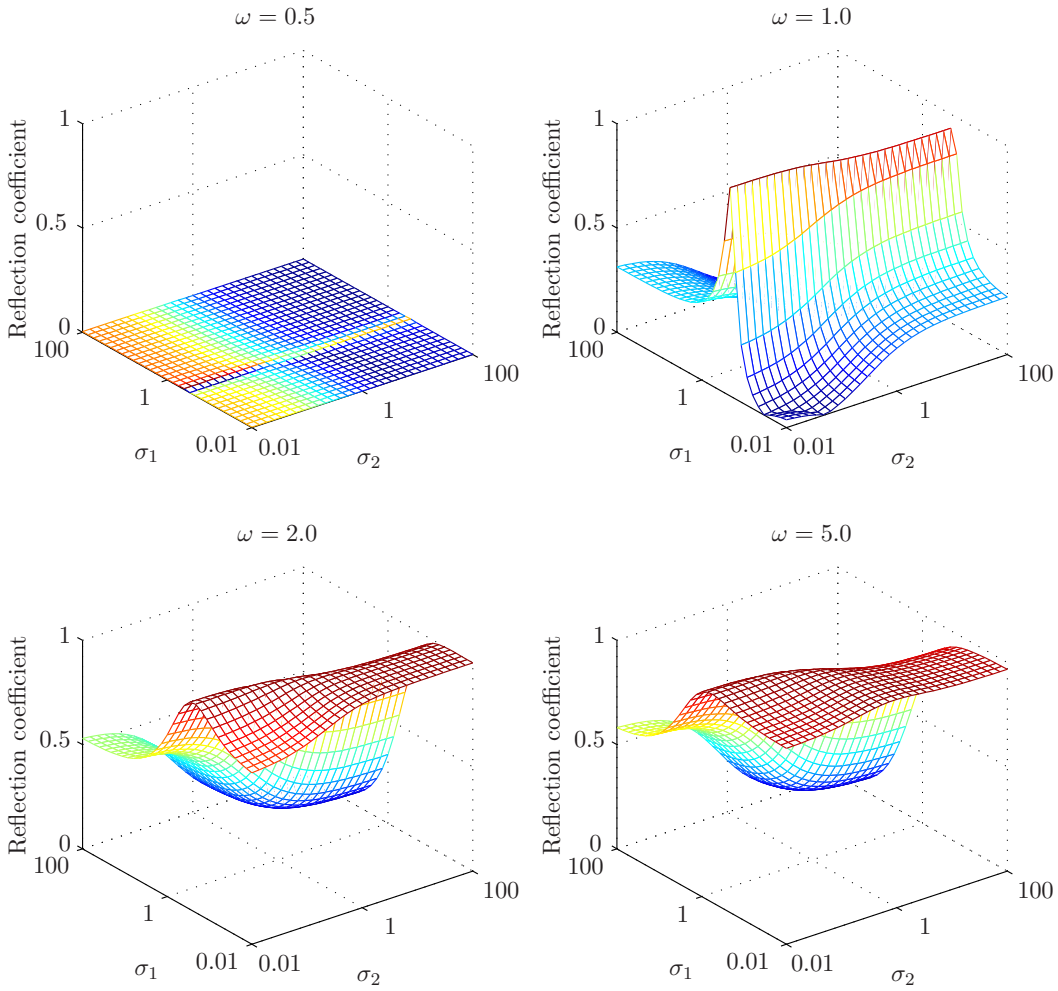

Figure 6: Reflection coefficient as a function of the spring constants for frequency $\omega = 0.5, 1.0, 2.0, 5.0$, when the incident angle is zero. The axes σ_1 and σ_2 are in log-scale. The water depth is 2π and $l_\mathrm{r} = 1$.

5 Computation of solutions

As a result of the derivation in section 4, computation of surface displacement for given boundary conditions is reduced to forming and solving (29) then evaluating (28). Given the ratio of the characteristic lengths l_{r}, which determines the roots of the dispersion equations, the elements of $\mathbf{T}_{\sigma_1,\sigma_2}$ are completely determined by σ_1 and σ_2 as shown in (30). Therefore, apart from the minor numerical computation of inverting a 4×4 matrix in (29), the displacement (28) is directly determined by the parameters (σ_1, σ_2). Therefore (28) can be rewritten to emphasize this direct relationship in the following form:

$$\eta\left(y;\sigma_1,\sigma_2\right) = c_4^{\pm}\left(y\right) + \left(\mathbf{T}_{\sigma_1,\sigma_2}^{-1}\mathbf{v}\right) \cdot \begin{pmatrix} c_0^{\pm}\left(y\right) \\ c_1^{\pm}\left(y\right) \\ c_2^{\pm}\left(y\right) \\ c_3^{\pm}\left(y\right) \end{pmatrix},$$

where $\cdot$ denotes inner product.

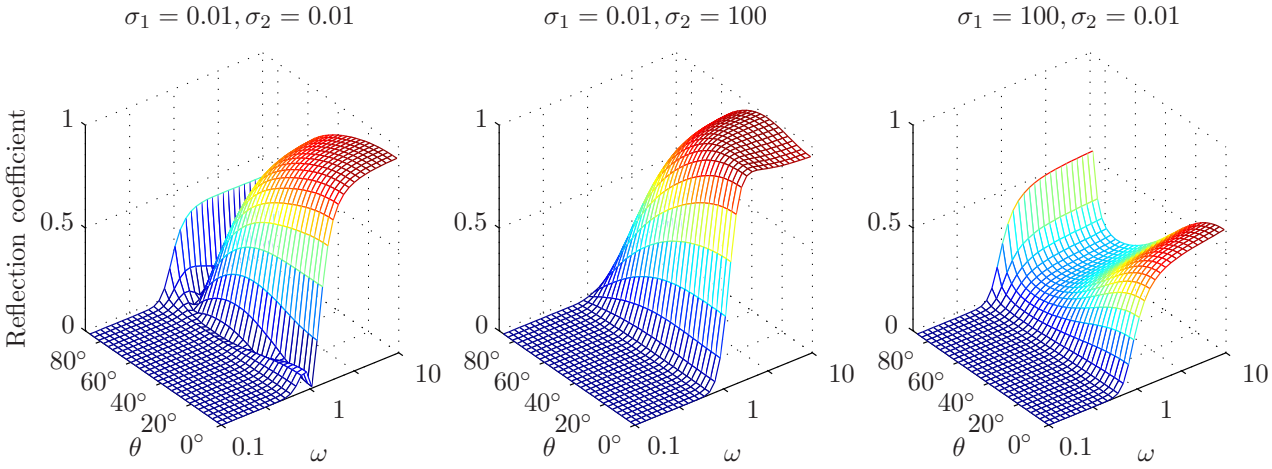

Figure 7: Reflection coefficient as a function of normalized frequency ω and incident angle θ, for various combinations of the spring constants. The axes ω is in log-scale. The water depth is 2π and $l_{\mathrm{r}} = 1$.

Figure 5 shows the four singular values of $\mathbf{T}_{\sigma_1,\sigma_2}$ as a function of ω for three choices of σ_1 and σ_2. The singular values stay virtually unchanged for $\omega < 0.7$ regardless of the values of the spring constants, that is, the crack is invisible to the waves. We note that this low-frequency regime is unchanged from the case of free-edge conditions shown in figure 3. When the connection is loose, $\sigma_1 = \sigma_2 = 0.01$, there are only two non-zero singular values. The system is nearly reduced to two identical semi-infinite ice sheets with free-edge conditions. In the other extreme when σ_1 and σ_2 are large, all four singular values are close to 1 and change little over the frequency range. In this case the ice sheets are acting almost as one piece, thus there is little reflection of waves.

Figure 6 shows the reflection coefficient as a function of the spring constants when $l_{\mathrm{r}} = 1$ and $\theta = 0$. It shows again that varying transitions conditions makes little difference to the wave propagation in the low frequency range. Both the vertical and the rotational springs are influential to the reflection of the waves at higher frequencies. When both σ_1 and σ_2 are small or large, both springs affect the reflection coefficient equally at all frequencies. However, in an intermediate range the vertical spring constant σ_1 induces

more rapid variation to the reflection coefficient than σ_2 does. In particular, the reflection coefficient changes rapidly near $\sigma_1 = 1$ at $\omega = 1$, which may be be useful in determining σ_1 and σ_2 from field measurements of the reflection coefficient.

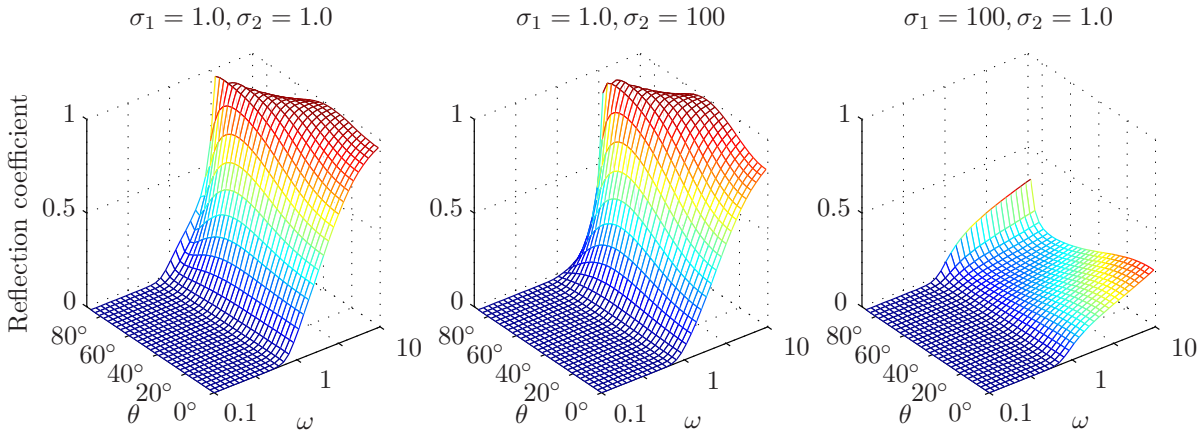

Figure 8: Reflection coefficient as a function of normalized frequency and incident angle with different combinations of the spring constants from those in figure 7.

Figures 7 and 8 show the reflection coefficient as a function of normalized frequency and incident angle. When $\sigma_1 = \sigma_2 = 0.01$ characterizing loose connection in figure 7, the reflection coefficient shows slight change from the free-edge case in figure 3. The sharp dip shown in figure 3 disappears as the connection at the crack becomes stronger. This *dip* feature has been observed in other papers (see [6, 3, 19]) for open crack cases. The reflection coefficient changes its character as the connection changes from one extreme to the other. Both figures 7 and 8 show that the rigidness of the bending and the vertical connection at the crack acts in a completely different manner. The reflection coefficient maintains its feature under varying bending connection rigidity, but changes completely as displacement connection rigidity varies. All figures show that the ice sheets act as one piece at low-frequencies regardless of the connection conditions or the incident angles.

A further study is required to find a relationship between physical composition of ice cracks and (σ_1, σ_2). However, it is possible to speculate what the values of (σ_1, σ_2) may mean in reality. For example, when σ_1 is small and σ_2 is large in figure 7, the ice sheets may be squeezed tightly and not be able to bend from each other but able to slide at the crack. The other extreme may be that the crack is partly re-frozen and is able to bend but unable to slide, corresponding to σ_1 is large and σ_2 is small. Figures 6, 7 and 8 indicate that the amount of slippage at the crack, which affects the displacement connection rigidity (σ_1), may need more attention than rotational rigidity (σ_2).

6 Discussion

The W-H technique gives an analytic solution, which we can use to derive the direct relationship between the edge boundary conditions and the wave trnasmission/reflection across a crack. The influence of the varying connection rigidity on the wave propagation is made clear by the solution. It suggests that the parameters σ_1 and σ_2 are sensible tools to describe the crack conditions. The reduction of the solution procedure to the matrix $\mathbf{T}_{\sigma_1,\sigma_2}$ enables us to study the wave propagation qualitatively without computing the

whole solution, rather we need only look into the matrix. One example of such analysis is to focus on the singular values of $\mathbf{T}_{\sigma_1,\sigma_2}$.

The reduction made possible by Liouville's theorem rests, ultimately, on conservation of energy at the interface between the two ice sheets (or at the edge of an ice sheet in the single-plate case). That connection was made explicit in earlier applications of the W-H technique where the order of transforms for $|\alpha| \to \infty$ (see section 3.2) were determined by the singularity possible at $y = 0$ that conserves energy (see e.g. [5]). (We have avoided this complication by treating the case of finite depth and using the location of the isolated roots of the dispersion equations.) Therefore the reduction of an infinite set of coefficients to a finite set achieved by applying Liouville's theorem is applicable at each of many interfaces when the wave propagates across multiple cracks. We found this observation useful in understanding and simplifying the solutions derived by Tkacheva [18] for propagating across finite interfaces. The reduction also provides a route to generalizing these solutions to more complex geometries. In principle, the explicit reduction given here provides a useful method for giving an exact finite dimensional representation of wave propagation problems in complex composite ice covers, where all junctions conserve energy. This is an intriguing advance over finite numerical discretization methods that necessarily introduce approximations.

References

[1] N.J. Balmforth and R.V. Craster, "Ocean waves and ice sheets" J. Fluid Mech. 395, 89–124 (1999).

[2] G.F. Carrier, M. Krook and C.E. Pearson, Functions of a complex variable, theory and technique, SIAM, Philadelphia (2005).

[3] H. Chung and C.M. Linton, "Reflection and transmission of waves across a gap between two semi-infinite elastic plates on water" Q. J. Mech. Appl. Maths 58(1), 1–15 (2005).

[4] H. Chung and C. Fox, "Propagation of Flexural Waves at the Interface Between Floating Plates" Int. J. Offshore Polar Eng. 12, 163–170 (2002).

[5] D.V. Evans and T.V. Davies, "Wave-ice interaction" report 1313, Davidson Laboratory, Stevens Institute of Technology, Hoboken (1968).

[6] D.V. Evans and R. Porter, "Wave Scattering by Narrow Cracks in Ice Sheets Floating on Water of Finite Depth" J. Fluid Mech. 484, 143–166 (2003).

[7] C. Fox, Scaling Laws for Flexural Waves in Floating Ice in IUTAM Symposium on Scaling Laws in Ice Mechanics and Ice Dynamics Fairbanks, Alaska, USA, 13-16 June 2000, Series : Solid Mechanics and Its Applications , Vol. 94, Dempsey, J.P. and Shen, H.H. (Eds.), (2002).

[8] C. Fox and H. Chung, "Harmonic Deflections of an Infinite Floating Plate" Department of Mathematics, University of Auckland, Report Series, 485 (2002) Avialable at www.math.auckland.ac.nz/Research/Reports/

[9] C. Fox and V.A. Squire, "On the Oblique Reflexion and Transmission of Ocean Waves at Shore Fast Sea Ice" Phil. Trans. R. Soc. Lond. A 347, 185-218 (1994).

[10] R.V. Goldstein and A.V. Marchenko, "The diffraction of plane gravitational waves by the edge of an ice cover" J. Appl. Mech. (Prikl. Matem. Mekhan) 53(6), 731–736 (1989).

[11] A.L. Kohout and M.H. Meylan, "An elastic plate model for wave attenuation and ice floe breaking in the marginal ice zone" J. Geophys. Res. 113, C09016, doi:10.1029/2007JC004434 (2008).

[12] J.B. Lawrie and I.D. Abrahams, "An Orthogonality Relation for a Class of Problems with High-Order Boundary Conditions; Applications in Sound-Structure Interaction" Q. J. Mech. Appl. Maths 52(2), 161–181 (1999)

[13] A.V Marchenko, "Flexural-gravity wave diffraction at linear irregularities in sheet ice" Fluid mech. 32, 548–560 (1997).

[14] B. Noble, Methods based on the Wiener-Hopf technique for the solution of partial differential equations, Pergamon Press, London (1958).

[15] I.H. Shames and C.L. Dym, Energy and finite element methods in structural mechanics, si units ed., Hemisphere Publishing Corporation, Bristol (1991).

[16] V.A. Squire, J.P. Dugan, P. Wadhams, P.J. Rottier and A.J. Liu, "Of ocean waves and sea ice" Annu. Rev. Fluid Mech. 27, 115-168 (1995).

[17] L.A. Tkacheva, "Scattering of surface waves by the edge of a floating elastic plate" Journal of Applied mechanics and Technical Physics 42(2), 638–646 (2001).

[18] L.A. Tkacheva, "Diffraction of surface waves at floating elastic plate" 17th International Workshop On Water Waves and Floating Bodies, Peterhouse, Cambridge, UK, April (2002).

[19] T.D. Williams and V.A Squire, "Scattering of flexural gravity waves at the boundaries between three floating sheets with applications" J. Fluid Mech. 569, 113–140 (2006).